

# Progress in scanning probe microscopy: High resolution force microscopy and spectroscopy

Ragnar Erlandsson<sup>\*,†</sup> and Peter Apell<sup>\*\*</sup>

<sup>\*</sup>Laboratory of Applied Physics, Department of Physics and Measurement Technology, Linköping University, S-581 83 Linköping, Sweden

<sup>\*\*</sup>Department of Applied Physics, Chalmers University of Technology and Göteborg University, S-41 296, Göteborg, Sweden

During the last few years the Atomic Force Microscope (AFM) has become capable of routinely obtaining atomic resolution when operated with a vibrating cantilever (ac-mode). Local measurement of the tip-sample force (force spectroscopy) is a powerful tool for investigations of contact phenomena at the atomic scale that are important in fields like friction, tribology, atom manipulation and chemical bond formation. This paper reviews several aspects of the AFM technique such as tip-surface forces, force sensors, operation modes and contrast effects. A study of the Si(111)7 × 7 reconstruction is presented as an example of high resolution AFM imaging.

## 1. Scanning probe microscopy – An introduction

The Atomic Force Microscope (AFM)<sup>1</sup>, which is the topic of this article, belongs to the family of techniques that are based on the concept introduced with the invention of the Scanning Tunnelling Microscope (STM) almost twenty years ago<sup>2</sup>. This class of instruments, often called Scanning Probe Microscopes (SPMs), uses the interaction between a sharp tip and the surface to obtain a topographic representation of the sample, as illustrated in Figure 1. Even though this idea had been demonstrated earlier<sup>3</sup>, the invention of the STM was the breakthrough that initiated the development of the whole range of SPM instruments available today, as it demonstrated the capability to resolve individual atoms. This remarkable performance for a technique that uses mechanical components to trace the contours of a surface is related to the extreme separation dependence of the tunnelling current between the tip and the surface for separations below 10 Å. As the current increases approximately one order of magnitude as the separation is decreased by 1 Å, atomic resolution is possible since the interaction will be confined to a single atom at the tip apex. By measuring the tunnelling current and using it as the control parameter for a feedback system it is thus possible to obtain traces corresponding to constant tunnelling current as the tip is scanned over the surface.

The surface maps obtained in this way are often regarded as a topographic representation of the sample, as they in many cases show the position of the individual atom cores. It should, however, be kept in mind that the tunnelling current has a complex relation to the electronic structure of both the surface and the tip. These effects have been investigated extensively, and the present understanding of the contrast mechanism in STM makes it possible to extract valuable information concerning the electronic structure on the local scale. An in-depth treatment of the SPM techniques and their applications can be found in the literature given in ref. 4.

These unique properties of the STM, the atomic resolution and the sensitivity to electronic structure, quickly made the method a widespread tool for surface science investigations of various kinds. Another aspect of the invention of the STM, as important as the performance of the instrument itself, was that it initiated the development of other techniques based on the same concept but using other kinds of interaction to track the surface contours. A great variety of SPM instruments have been demonstrated using various kinds of forces<sup>5</sup>, capacitance<sup>6</sup>, thermal conductance<sup>7</sup>, ion conductance<sup>8</sup>, acoustical interaction<sup>9</sup> and optical interaction<sup>10</sup>, just to mention a few. Of all the techniques descendent from the STM, it is the AFM (also called Scanning Force Microscope, SFM) that has been most widely used as it allows determination of the topography of almost all kinds of surfaces and can operate in different media like air, liquid and vacuum. The evolution of the AFM has, however, been very different compared to the STM, as it is the versatility of force microscopy that has been its main advantage rather than the ability to obtain extreme resolution. Even though the AFM was invented in 1986, it was only a few years ago that true atomic resolution comparable with the STM could be obtained. The reason for this is the difference in tip-surface interaction for the two techniques and technical complications related to the measurement of small interaction forces. In this paper the basic properties of the AFM techniques with focus on high resolution measurements in ultrahigh vacuum (UHV) will be described and exemplified by measurements from our laboratory.

<sup>†</sup>For correspondence. (e-mail: rag@ifm.liu.se)

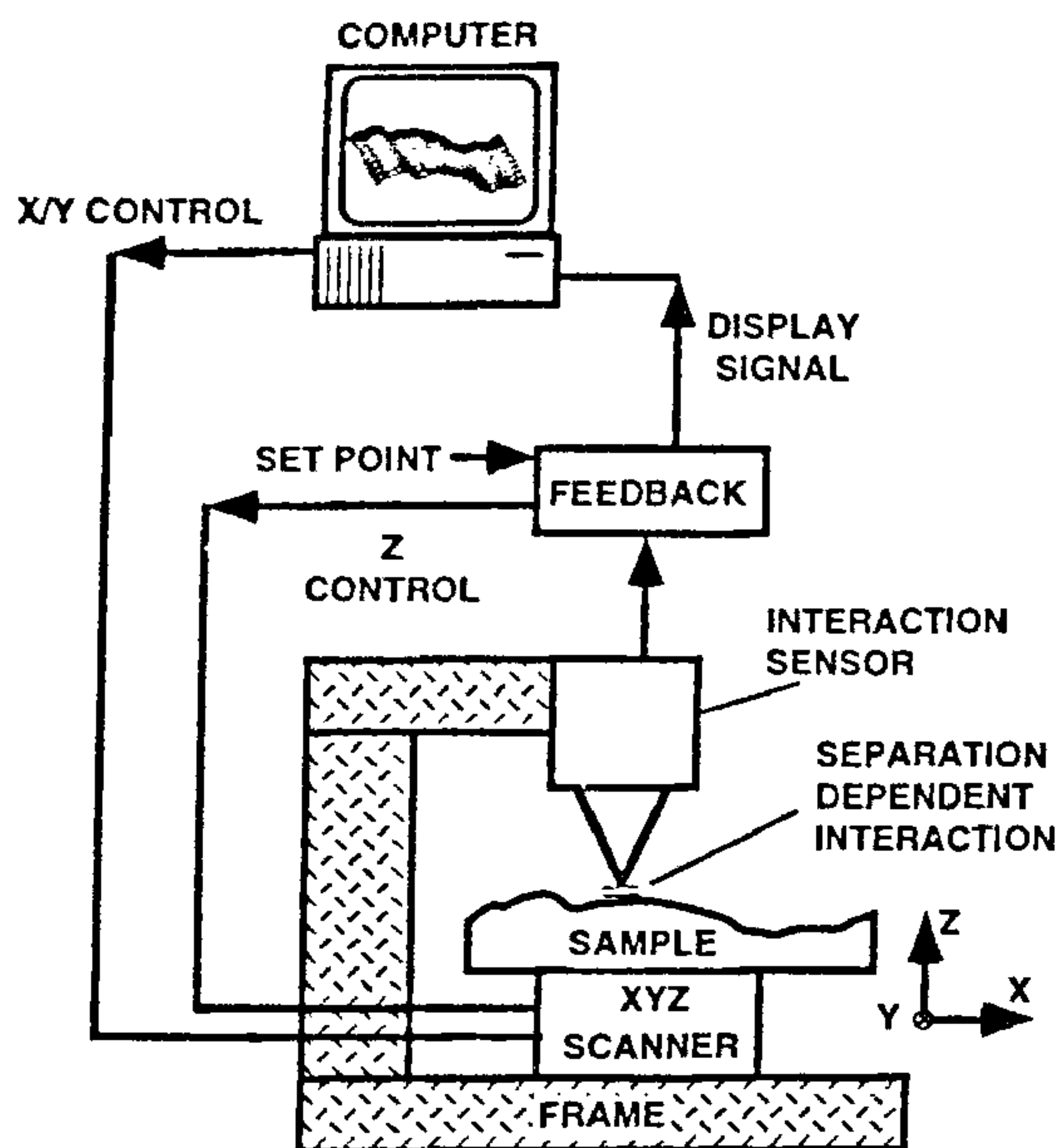


**Figure 1.** The common principle of scanning probe microscopes. By measuring a distance dependent tip–surface interaction, which could be a tunnelling current or an interaction force, and use this signal as control parameter for a feedback circuit controlling the z-position of the sample, the tip to sample separation will remain constant. As the tip is scanned over the surface, the  $z = f(x, y)$  plot will generate a topographic image of the sample provided the interaction does not vary due to other effects.

## 2. The force interaction

### 2.1. Origin of tip–surface forces

The forces between the tip and the surface are normally separated into short-range and long-range forces (Figure 2). The long-range force which always exists over a vacuum gap is the van der Waals interaction<sup>11</sup>. Assuming that this force is additive and can be described in the non-retarded regime, a simple analytical expression describing the interaction between a surface and tips of various geometries can be derived<sup>12</sup>. For a vacuum gap, the van der Waals force is always attractive and the separation dependence is strongly influenced by the tip geometry. The van der Waals force between the tip and the sample can be estimated within the Hamaker theory<sup>13</sup>, the main assumption being the pairwise additivity of tip and sample contributions to the total interaction. However, using the so-called Derjagin approximation<sup>14</sup> one can go a step further. For arbitrary but smooth geometries it enables one to separate the interaction in two parts. One is a spatial part only related to the geometric aspects of the interacting systems and the other part is related to the electronic response properties of the tip and sample going beyond pairwise interaction. This is very convenient since the latter can be calculated once

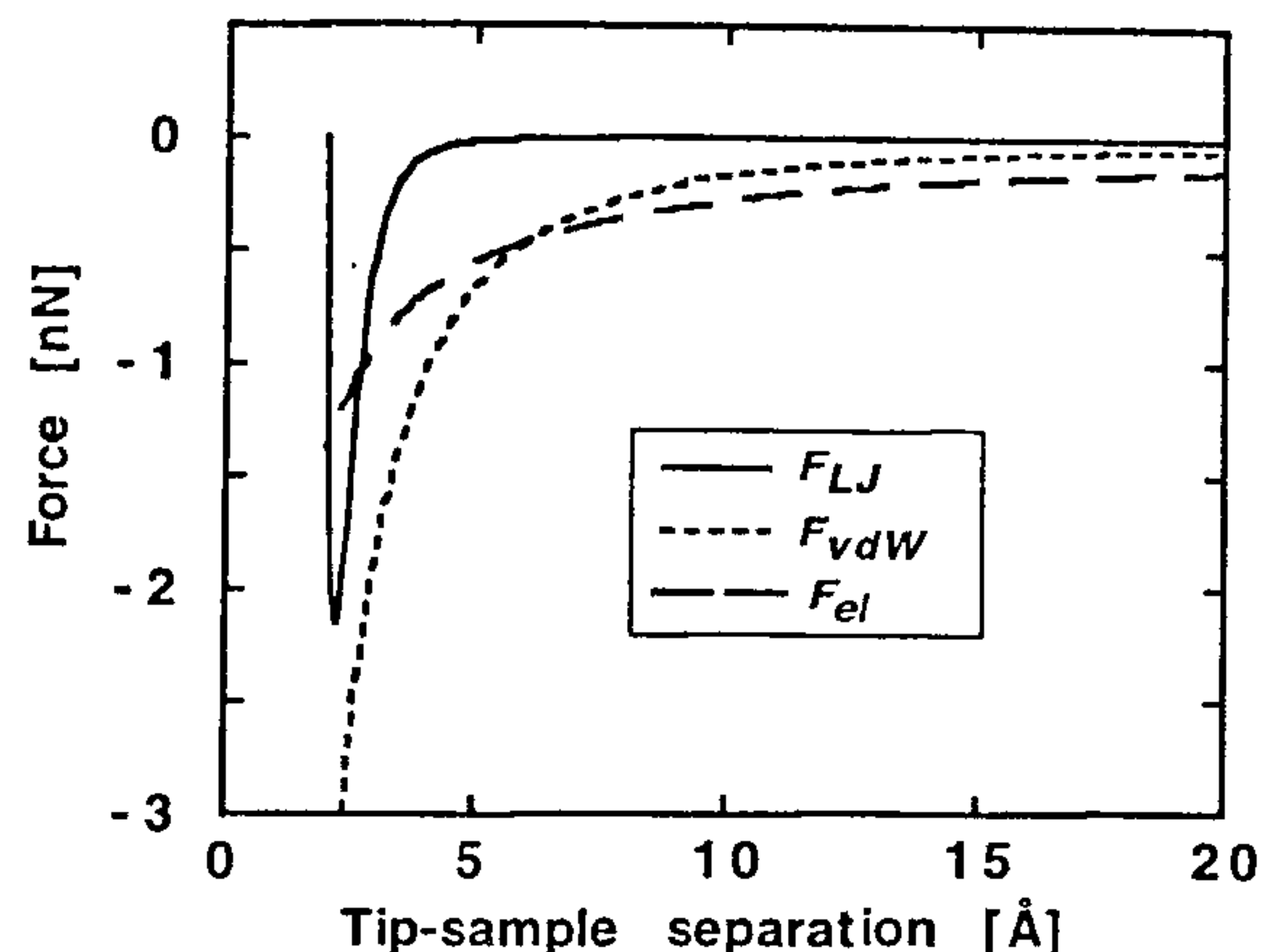


**Figure 2.** Separation variation of the van der Waals force ( $F_{vdW}$ ) and the electrostatic force ( $F_{el}$ ) for a spherical tip compared with the Lennard–Jones force ( $F_{LJ}$ ) for a bond with equilibrium separation  $\sigma = 2 \text{ Å}$  and binding energy  $E_b = 1 \text{ eV}$ . Tip radius and bias voltage are  $R = 100 \text{ Å}$  and  $U = 1 \text{ V}$ , respectively. The expressions used for the forces are

$$F_{vdW, \text{sphere}} = -\frac{AR}{6d^2},$$

$$F_{el, \text{sphere}} = -\frac{\pi\epsilon_0 U^2 R}{d},$$

$$F_{LJ} = -12\frac{E_b}{\sigma} \left[ \left( \frac{\sigma}{d} \right)^7 - \left( \frac{\sigma}{d} \right)^{13} \right],$$

where  $d$  is the separation,  $A$  is the Hamaker constant and  $\epsilon_0$  the dielectric constant for vacuum.

and for all for a given combination of material using the most sophisticated materials codes around<sup>15</sup>.

In ac-mode force microscopy the main quantity of interest is the force gradient  $F' = \partial F / \partial d$  which can be expressed as

$$F' = 4\pi R_{\text{eff}} \frac{C_2}{d^3}, \quad (1)$$

within the Derjagin approximation. The combined effective radius  $R_{\text{eff}}$  of the tip and sample is given by<sup>16</sup>:

$$\frac{1}{R_{\text{eff}}^2} = \left( \frac{1}{R_{a1}} + \frac{1}{R_{b1}} \right) \left( \frac{1}{R_{a2}} + \frac{1}{R_{b2}} \right) + \sin^2 \theta \left( \frac{1}{R_{a1}} - \frac{1}{R_{a2}} \right) \left( \frac{1}{R_{b1}} - \frac{1}{R_{b2}} \right), \quad (2)$$

where  $\theta$  is an angle between the surface plane coordinate systems of the tip and sample ( $a$  and  $b$ ). ( $R_{a1}$ ,  $R_{a2}$ ) and ( $R_{b1}$ ,  $R_{b2}$ ) are the principal radii of curvature of the two surfaces facing each other.  $C_2$  is the regular van der

Waals interaction coefficient between two planar surfaces. It goes beyond the pairwise additivity in the Hamaker theory but, for dilute samples it reduces to  $A/12\pi$ , where  $A$  is the so-called Hamaker constant.

To make results more transparent let us look at an example of a sphere of radius  $R$  interacting with a cylinder of radius  $L$ . Then  $R_{a1} = R_{a2} = R$ ,  $R_{b1} = L$  and  $R_{b2} = \infty$ . This gives a resulting radius of curvature

$$R_{\text{eff}} = R \sqrt{\frac{L}{R+L}}.$$

Hence in this case:

$$F' = 4\pi R \sqrt{\frac{L}{R+L}} [C_2 / d^3], \quad (3)$$

which for a large cylinder  $L \gg R$ , and in the dilute limit, reduces to the well-known result for a sphere of radius  $R$  a distance  $d$  from a planar surface

$$F = \frac{AR}{6d^2}, \quad (4)$$

expressing it in terms of the force instead.

Other long-range forces are the electrostatic and magnetic interactions, but these are specific to the experimental conditions. For a conducting tip-sample system, the electrostatic force is always attractive, and can exist also for zero bias voltage due to the contact potential difference between the tip and the surface materials. The electrostatic force has the advantage that it can easily be manipulated by the operator and can be used to obtain information about the size and shape of the tip<sup>17</sup>. Electrostatic Force Microscopes (EFMs) specifically designed to measure the electrostatic interaction<sup>5</sup>, can be used to measure charge distributions in insulators<sup>18</sup>, variations in surface contact potential and capacitance gradients on the sample surface. Magnetic forces are normally not encountered in AFM experiments that are not specifically designed for this purpose, as they require a tip of magnetic material that should be magnetized in a well-defined manner. AFMs specifically tailored for magnetic measurements are referred to as Magnetic Force Microscopes (MFMs) and will not be treated here. A detailed description of the MFM technique can be found in Grütter *et al.*<sup>19</sup>.

The short-range force requires a quantum mechanical treatment, and according to the Hellman-Feynman theorem<sup>20</sup>, this force can be obtained from a purely classical electrostatic calculation once the electronic charge density has been obtained by a self-consistent quantum mechanical procedure. This short-range force can be divided into two components,  $F_{\text{ion}}$  which represents the repulsive Coulomb force between the ion cores, and  $F_{\text{el}}$  which represents the interaction between the valence electrons associated with chemical bonding<sup>21</sup>. A unified treatment of the short-range force interaction and the

tunnelling interaction is given by Chen<sup>22</sup>, where it is shown that a direct relation can be obtained between the tunnelling current and the attractive short-range force for metallic systems. For a simple analytical estimation of the short-range forces, the Lennard-Jones potential<sup>23</sup> or the Morse potential<sup>24</sup> is often used. The Lennard-Jones force for a typical binding energy and bond separation is illustrated in Figure 2 together with the van der Waals and electrostatic long-range forces corresponding to tips with spherical geometry. The analytical expressions for the plotted forces are given in the caption to Figure 2.

For instruments operating under ambient conditions there is the additional complication of a thin liquid film covering the sample surface, forming a liquid bridge at separations of 50–100 Å, that will give rise to an attractive force due to the surface tension in the meniscus<sup>25</sup>. As this effect makes force measurements in air difficult, precise studies of the tip-surface interaction normally require good vacuum or that the measurement takes place in liquid.

## 2.2. Forces during STM operation

When the tip in a STM instrument moves over the surface at a separation of typically 2–10 Å, there will always be a force interaction over the gap junction. For hard materials this might have no consequence, but it was early recognized that it gave rise to anomalous high corrugation amplitudes for soft materials like graphite. This effect could not be explained by the tunnelling theory but was attributed to the elastic deformation of the surface that varied as a function of the tip position<sup>26</sup>. Investigations of the tunnelling barrier, where the tunnelling current is measured as a function of separation, also gave anomalous results for separations below a few Å, which can be understood by elastic deformations due to tip-surface forces<sup>27</sup>. Early measurements of the interaction force during tunnelling were made by observing the resonance frequency variations of a cantilever beam on which the tunnelling tip was mounted, indicating that metallic adhesion forces dominated for separations within a range of 2 Å (ref. 28). A spectacular use of force effects during STM operation are the manipulation experiments where individual atoms are moved into defined crystal positions<sup>29</sup>.

## 3. The AFM instrument

### 3.1. The force sensor

Much of the technology used in the AFM is identical to that developed for the STM, such as sample motion using piezoelectric transducers, feedback controller, image

handling, vibration damping, etc. and will not be explicitly treated here. The critical part of the AFM is the force sensor which transforms the force interaction over the tip-sample junction to an electrical signal that can be handled by the feedback electronics. This is done by having the tip mounted on a flexible cantilever combined with a deflection sensor that can measure the cantilever motion as the tip interacts with the surface. As the tip is a part of the force sensor, it is normally the sample that is moved with a piezoelectric transducer in the AFM. In the first AFM instrument, a tip close to the backside of the cantilever was used to detect the motion as in a STM but modern designs use optical techniques to measure the cantilever deflection as shown in Figure 3.

The most common optical detection scheme uses light from a solid state laser that is focused on the backside of the cantilever which reflects the beam into a position sensitive detector<sup>30</sup>. As the cantilever deflects, the beam moves over the multi-segment detector and an electrical signal corresponding to the difference of the photocurrents from the segments is generated. By using a photo-detector that is sensitive to the beam position in two directions, it is possible to detect the motion of the cantilever both perpendicular to the sample and the torsion of the cantilever induced by frictional forces, as

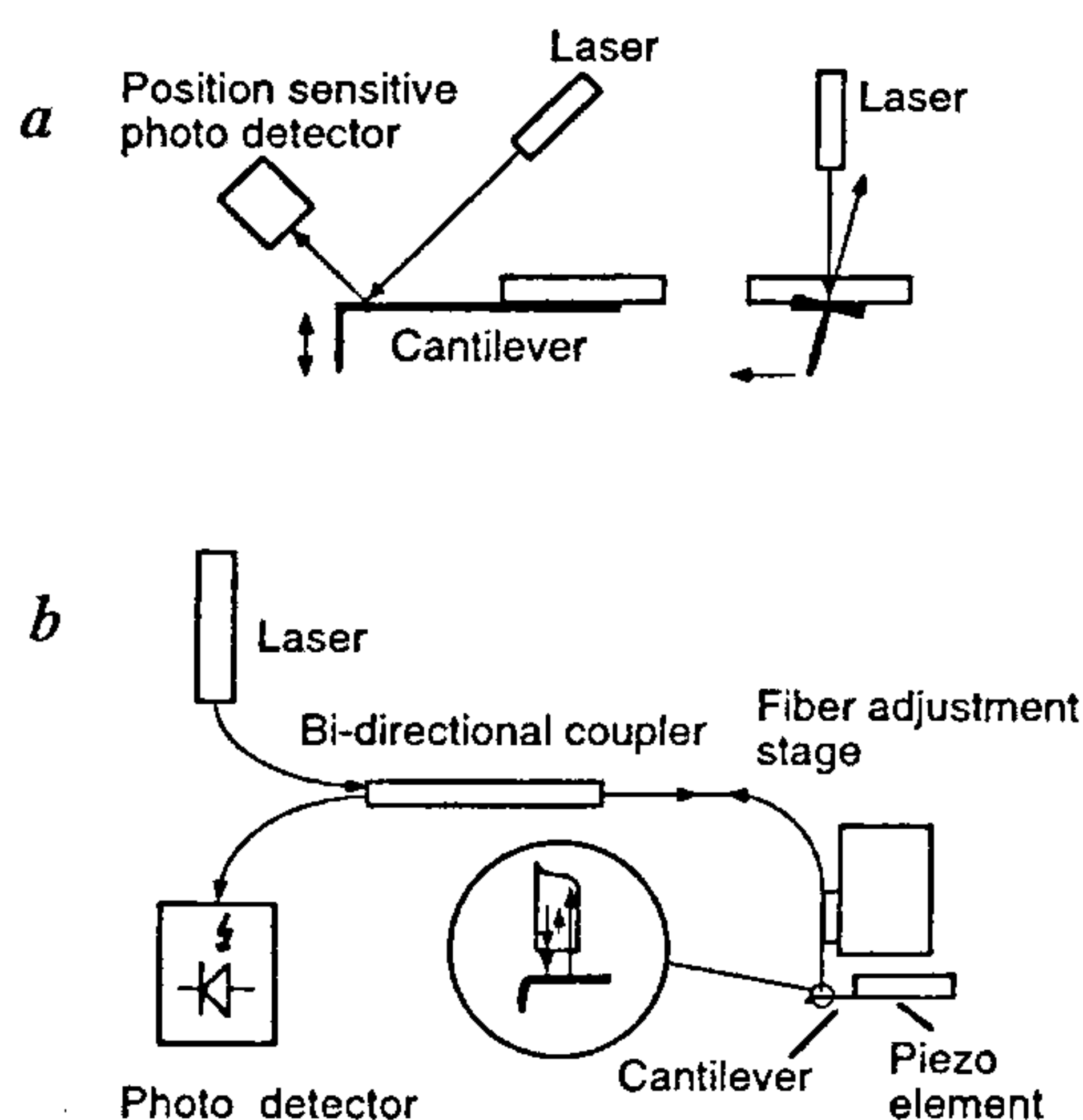


**Figure 3.** The two most common methods to detect cantilever deflection are shown. *a*, The beam deflection detector is normally used for instruments operating under ambient conditions. Measurement of frictional forces by using a photo-detector that is sensitive in the direction corresponding to the torsion of the cantilever is illustrated; *b*, In the fiber optic interferometer, the beam reflected from the cantilever surface interferes with the beam reflected at the end facet of the fiber which gives an interference cavity that is typically 1  $\mu\text{m}$  long. As the fiber is the only part of the sensor that has to reach the cantilever, this method is well-suited in cases where access is a problem.

shown in Figure 3. AFM instruments operating in UHV often use deflection sensors based on interferometry<sup>31</sup>, as the only part that has to be inserted into the vacuum chamber is an optical fiber. This type of sensor also has the advantage that the wavelength of light can be used as a calibration for the cantilever motion. The cantilever and tip are normally integrated in one unit and can be obtained commercially from several sources, but can also be individually made by bending and electrochemically etching a thin metal wire, as we often do in our laboratory. The cantilever is characterized by its spring constant  $k$  and resonance frequency  $f_{\text{res}}$ . A high value of  $f_{\text{res}}$  is normally desirable to minimize the sensitivity to vibrations, while the optimum value of  $k$  is determined by the operation mode of the instrument as described here. As the AFM is often used for lower resolution measurements than the STM, a small cone angle of the tip is an important parameter in order to reproduce sharp edges and narrow recessions in the sample. The general problem of tip convolution effects is illustrated in Figure 4, which shows a  $\text{SiO}_2$  surface covered with palladium islands imaged with tips of different quality. This type of artifacts, that are common to all SPM techniques, can to some extent be corrected for by computer manipulation of the topographic data<sup>32</sup>.

### 3.2. Operation modes of the AFM

**3.2.1 Contact, non-contact, dc and ac-modes:** The operation of the AFM can be characterized as contact or non-contact, depending on whether the tip enters the repulsive force region or not. Another common distinction is whether the force is obtained directly from the static deflection of the cantilever, dc-mode, or if the proximity of the surface is sensed by detecting the change in resonance properties of an oscillating cantilever which is known as ac-mode or dynamic AFM. Instruments operating in the ac-mode require that the cantilever is mounted on a piezoelectric transducer, and that the bandwidth of the deflection detector is high enough to measure at the cantilever resonance frequency that can be several hundred kHz. A block diagram of an AFM instrument capable of operating in both modes is shown in Figure 5.

**3.2.2 DC-mode operation:** The original method of operating the force microscope was the contact dc-mode, where the bending of the cantilever due to the repulsive interaction was kept constant by the feedback system, which means that the traced contours correspond to lines of constant repulsive force. This requires a low cantilever spring constant in order to have a high force sensitivity and avoid unnecessary damage to fragile samples. As it is also desirable to have a high resonance frequency of the cantilever, it implies that the effective

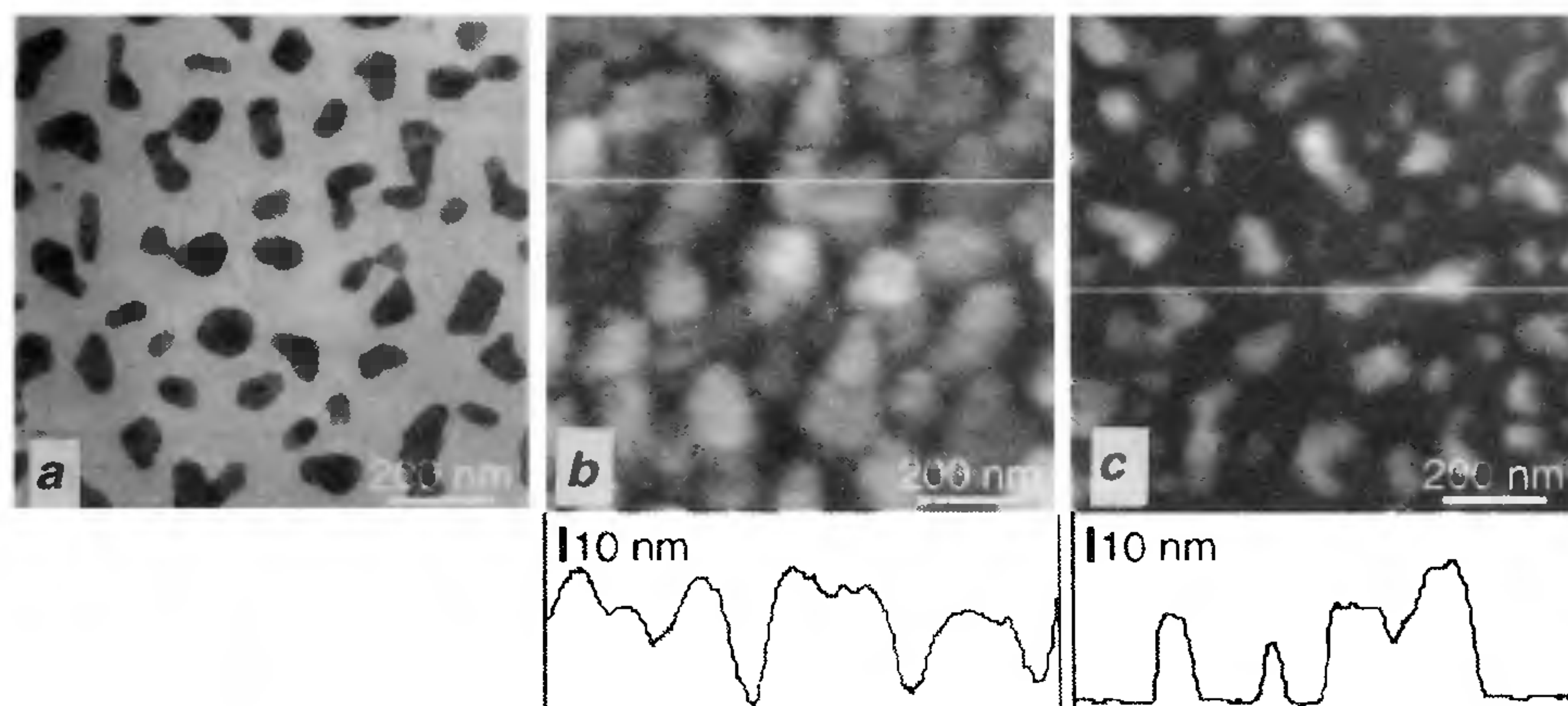


Figure 4. Three panels showing equal areas of Pd islands supported on SiO<sub>2</sub> imaged with (a) Transmission Electron Microscopy (TEM); (b) AFM with a dull and (c) a sharp tip, together with cross-sections in the AFM images. The image in *b* shows the characteristic repeated structures related to tip convolution, and the cross-section shows that the tip never reaches the SiO<sub>2</sub> support between the islands.

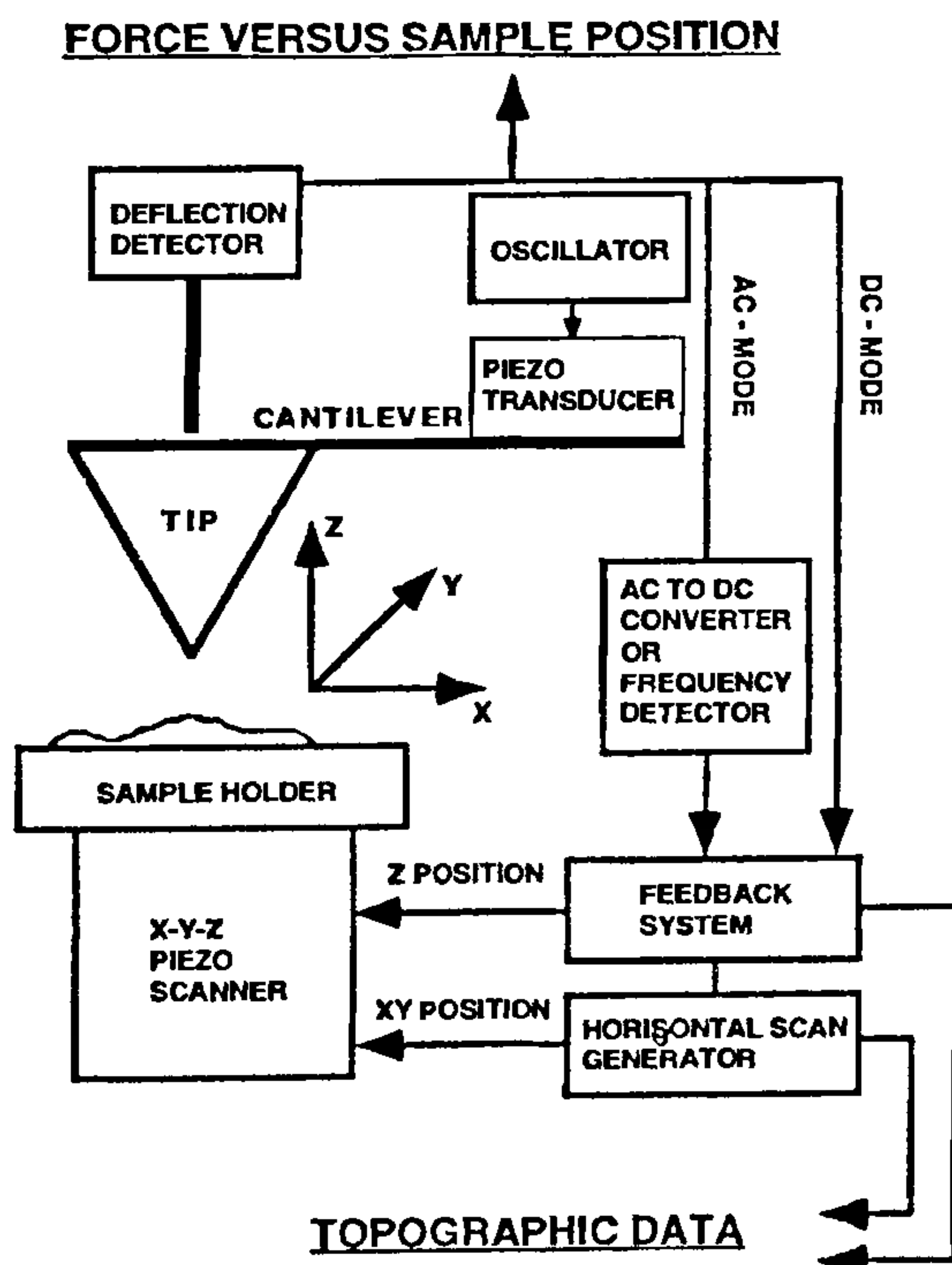


Figure 5. Block diagram of a force microscope equipped for both dc and ac-mode operation. The cantilever is mounted on a piezoelectric transducer so that it can be oscillated. The feedback system uses either the deflection signal (dc-mode) or the frequency signal (ac-mode) as the input parameter. By detecting the cantilever deflection as a function of sample position, dc-mode force curves are obtained.

mass should be low which means that the cantilever should be made as small as possible. Normally batch-fabricated cantilevers made from silicon or silicon nitride are used. In principle, this operation mode should be able to give very high resolution as the repulsive force between the tip apex atom and the sample,  $F_{ion}$ , has a range comparable to the tunnelling current. It has, however, turned out to be very difficult to obtain reliable atomic resolution, even though some convincing examples of truly atomically resolved images using dc-mode have been presented<sup>33</sup>. The problem with high resolution dc-mode imaging is illustrated in Figure 6 which shows that besides the localized repulsive contact at the apex atom, the tip is also subject to the long-range attractive van der Waals force that acts over a large part of the tip. Assuming a spherical tip shape, the van der Waals attraction will be proportional to  $1/d^2$ , where  $d$  is the tip-surface separation, while the spring force acting in the opposite direction varies linearly with the deflection. This leads to a mechanical instability which makes the tip jump into repulsive contact when the gradient of the attractive force equals the cantilever spring constant, as described in more detail next in the article. This phenomenon, which generally occurs for soft cantilevers, is known as 'jump to contact' or 'snap-in'. Even if the cantilever is perfectly stiff, it is expected that an intrinsic jump to contact should occur due to the elasticity of the tip and sample materials for separations of the order of 1 Å (ref. 34). Due to these effects, it is very difficult to precisely control the effective contact force, which has to be kept below approximately 1 nN if the integrity of the tip apex should be maintained during scanning in

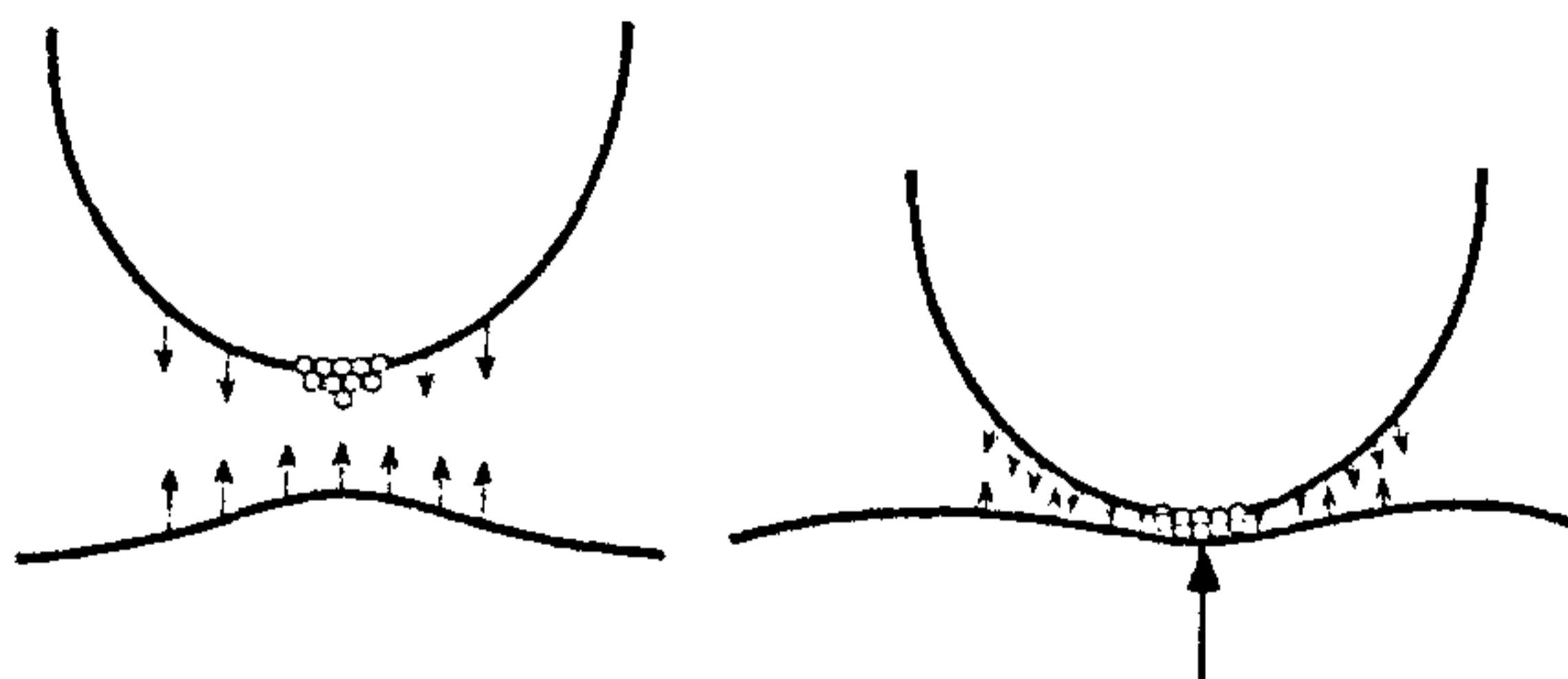


Figure 6. Long-range attractive force acting over a large part of the tip is balanced by the repulsive interaction at the apex atom cluster when operating in dc contact-mode.

order to allow atomically resolved imaging. One way to overcome this problem is to operate in the liquid phase, where a proper choice of the liquid can eliminate the van der Waals force. In principle, it is also possible to retract the cantilever base so that the spring force compensates for the long-range attraction which requires that the instrument is operated with the cantilever close to the snap-out point, which is technically difficult. Another problem related to dc contact-mode measurements is the influence of frictional forces generated as the tip is moved along the surface. These forces tend to move the tip parallel to the surface, inducing a torsion in the cantilever which can be interpreted by the deflection detector as a height variation. In several cases, especially when investigating layered materials, the frictional forces cause a lateral stick-slip motion of the cantilever with a periodicity of the atomic unit cell which is easily misinterpreted as 'atomic resolution'. By using an instrument that correctly measures the cantilever deflection parallel to the surface, the AFM can be used as a powerful tool for investigation of atomic scale friction<sup>35</sup>. An overview of the theory of friction forces related to AFM operation is given by Tománek<sup>36</sup>.

Due to the problem described above, the dc contact-mode has not evolved into a routine tool for atomically resolved imaging, and is increasingly superseded by ac-mode operation for lower resolution measurements in order to avoid artifacts related to the tip loading force. Imaging in the attractive force regime is normally not possible with dc-mode AFM, as it would require very soft cantilevers where the thermal noise would be too big, and the problems with the cantilever instability would be difficult to overcome.

**3.2.3 AC-mode operation:** When the cantilever is oscillated during the measurement and the effect on the oscillation due to the proximity of the surface is used for separation control, the instrument is operated in ac-mode. This turns out to be a practical method of controlling tip-sample separation, as the effective

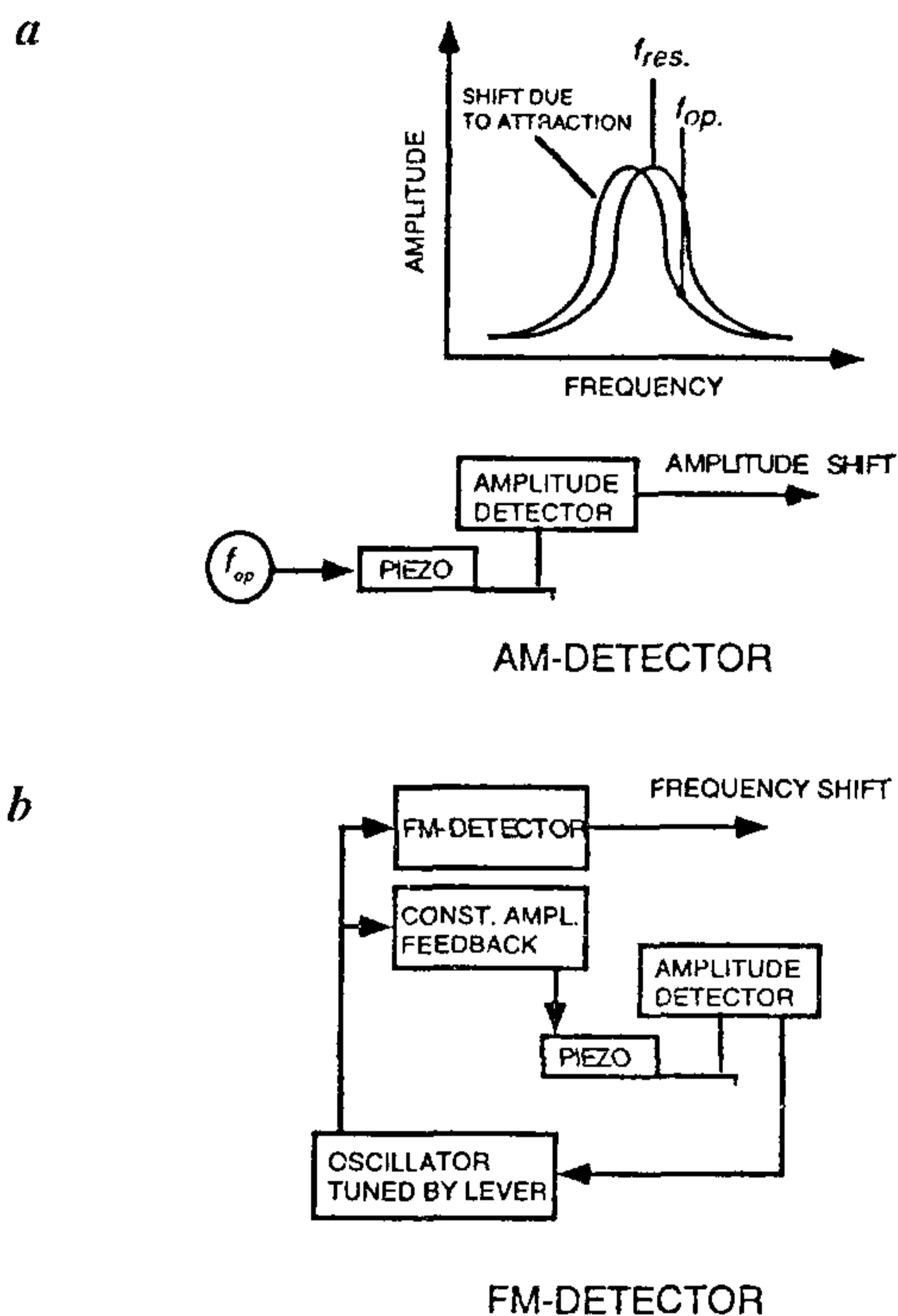


Figure 7. Two methods of detecting frequency shifts of the cantilever in ac-mode force microscopy: *a*, When using AM-detection the cantilever is oscillated at  $f_{op}$  which should correspond to the steepest part of the high frequency side of the cantilever resonance curve for maximum sensitivity. An attractive tip force will shift the resonance to a lower value, which gives a decreased oscillation amplitude; *b*, When using FM-detection the cantilever is the frequency determining element in an oscillator circuit. The frequency shift is obtained from an FM-detector.

resonance frequency of a cantilever is very sensitive to the force interaction. There are two common methods to detect this variation in  $f_{res}$ , as shown in Figure 7. When using AM-detection<sup>37</sup>, the cantilever base is oscillated with a constant frequency at or slightly above to the undisturbed resonance frequency (Figure 7*a*). As the oscillating tip enters the area where there is an attractive force gradient from the interaction with the sample, the effective spring constant will be lowered, and the oscillation amplitude is decreased. This amplitude variation is easily converted to a dc-signal that is used as a control parameter for the feedback electronics. This method is technically simple to implement, but both the sensitivity and speed depend on the quality factor (Q-value) of the cantilever resonance. As the measured amplitude shift is correlated to the frequency shift through the shape of the resonance curve, the interpretation of the obtained control signal is also complicated. These drawbacks can be overcome by using the FM-detection

technique (Figure 7 *b*), where the cantilever is used as the frequency determining element in an oscillator, and the frequency shift is directly converted to a control signal using an FM-detector<sup>38</sup>. The amplitude of the cantilever oscillation is normally kept constant during the interaction with the surface using an automatic gain control circuit. This method is inherently faster, and the set-point for the feedback can easily be adjusted to a pre-determined frequency shift.

While the cantilever deflection in dc-mode operation is directly related to the total force acting on the tip by Hook's law, the physical interpretation of the frequency shift in ac-mode measurements is considerably more complicated. The simplest case is the non-contact ac-mode operation with an oscillation amplitude so small that the gradient of the attractive interaction can be considered constant over the trajectory of the tip. In this case the frequency shift  $\Delta f$  is directly correlated to the force derivative through the expression  $\Delta f/f_{res} = F'/2k$ , where  $F'$  is the derivative of the interaction force. The corresponding image will in this case represent contours of constant force gradient. The condition that the oscillation amplitude is small in relation to the variation of the force gradient is, however, often not fulfilled. For high resolution imaging where the tip has to enter the short-range interaction regime, the oscillation amplitude will always be high compared to the local variation of the force gradient due to the short-range forces. In this case the cantilever cannot be treated as an harmonic oscillator, and the relation between the measured frequency shift and the force gradient has to be obtained from numerical simulations<sup>39</sup> or analytically by using perturbation theory<sup>40</sup>. The main advantage of ac-mode operation is the inherently high sensitivity, which makes it well-suited for investigating the weak long-range forces. The problem of cantilever jump-to-contact is also easier to overcome as the spring constants used, typically 10–100 N/m, are considerably higher than those used for dc-mode measurements, and that the condition for jump-to-contact to occur is different than in the dc-mode case<sup>40</sup>.

Force microscopes operating under ambient conditions often use a type of ac-mode operation with high cantilever amplitude, called tapping-mode or intermittent contact mode, where the tip goes into repulsive contact during each oscillation cycle. This has proven to be a very powerful technique as it avoids the tip being captured by the liquid film on the surface and gives considerably less force-induced-artifacts than dc contact-mode<sup>41</sup>. As the tip strikes the surface with a frequency of several hundred kHz during scanning, the problem associated with lateral forces is also small compared to dc contact-mode operation.

## 4. Force spectroscopy

### 4.1. Force interaction regimes

When the tip is placed at a point over the surface and the force interaction is measured as a function of sample position, the measurement is often referred to as force spectroscopy. The same distinction between dc and ac-mode operation as described earlier can be made in this case also. It is, however, only the dc-mode measurements that directly give the force versus separation data. If the tip moves far into the repulsive region, deformations will occur both in the tip and the surface, and the measurement can be characterized as a nanoindentation. This kind of measurement can be used to investigate the stepwise occurring rearrangements of the atoms due to the contact force which is related to tribology and contact mechanics and has been predicted by molecular dynamics simulations<sup>42</sup>. During these measurements a thin neck is often formed between tip and sample during the pull-off phase which can be used to study constriction effects showing quantized charge transport<sup>43</sup>.

Long-range forces are normally investigated with ac-mode measurements which give the variation of the force gradient as the primary information. The short-range forces related to chemical bonding, which give the contrast in atomically resolved AFM, are difficult to measure as dc-mode measurements require stiff cantilevers due to the strong force gradients, and ac-mode measurements give primary information that is difficult to translate into force versus separation curves. Some of the problems related to dc-mode measurements at close separation can be overcome by using the force-feedback detector, as described later in the article.

### 4.2. The dc-force curve

The normal dc-mode force experiment is done by measuring the deflection  $d$  of the cantilever as a function of the sample position to obtain the force from Hook's law,  $F = k \times d$ . The curves in Figure 8 *a* show the behaviour of the cantilever deflection as the sample is moved towards and then away from the tip. When the gradient of the attractive force reaches the same value as the cantilever spring constant, the tip will make a discontinuous jump to contact (from point 1 to point 2 in Figure 8). The origin of this phenomenon is shown in Figure 8 *b* where the interaction force is plotted as a function of tip-sample separation together with lines corresponding to the spring force of the cantilever with reversed sign for cantilever base positions corresponding to snap-in and snap-out events. From this curve it can be seen that the separation when snap-in occurs depends on the cantilever spring constant, and that the magnitude of the snap-out step is related to the depth of the force curve if

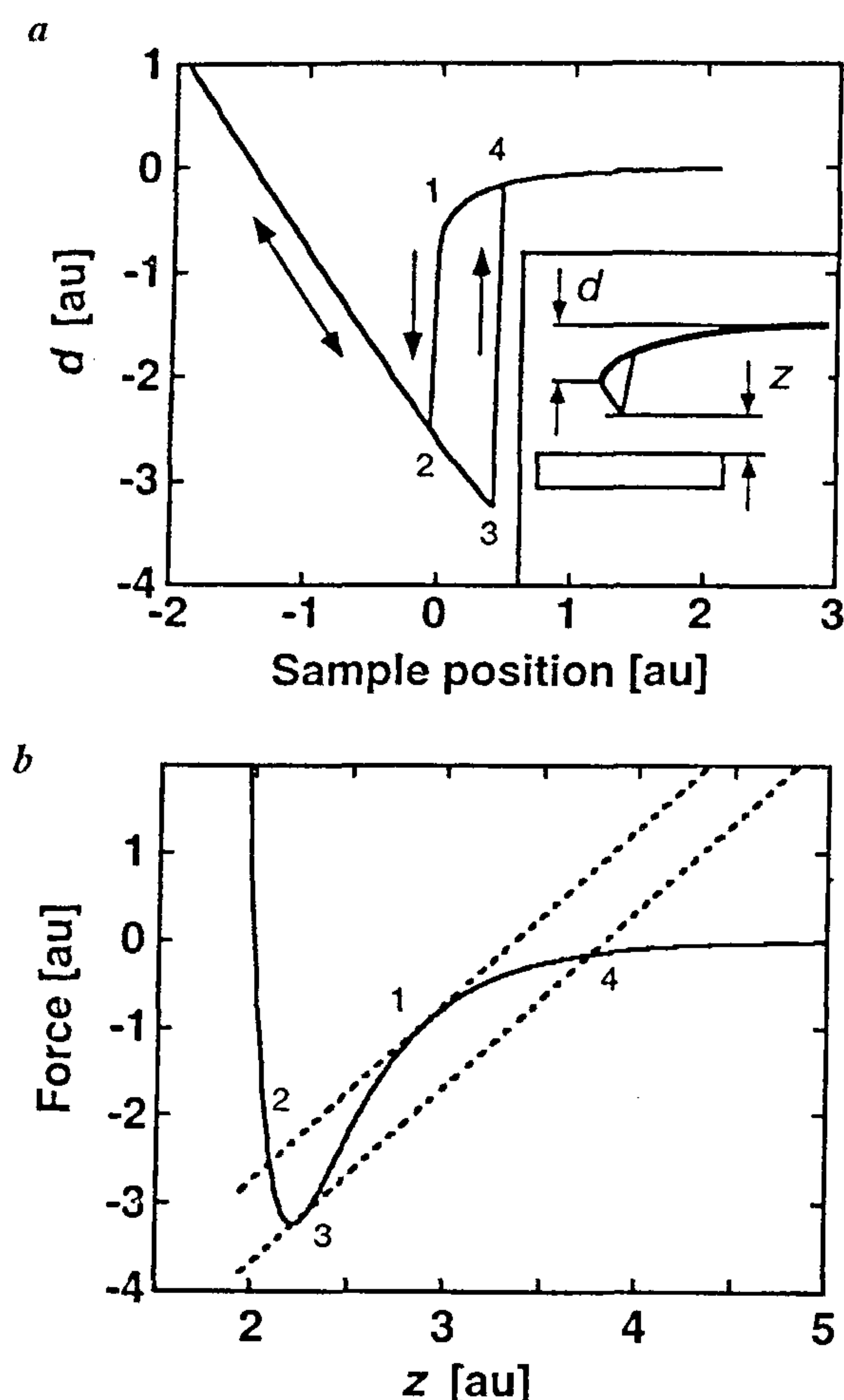


Figure 8. *a*, Principal behaviour of the cantilever deflection,  $d$ , as a function of sample position. Negative deflection corresponds to attraction. At point 1 the cantilever jumps into contact with the surface. The sample position where the cantilever jumps to contact is chosen as zero; *b*, Force versus separation  $z$  for the cantilever deflection curve in *a*. The hatched lines show the cantilever spring force with opposite sign for the sample positions where the tip jumps into contact (1–2) and is released (3–4).

the cantilever spring constant is significantly lower than maximum force gradient. In order to obtain an experimental curve that can be directly compared with the theoretical curves, one should transform the horizontal scale from sample position to tip–sample separation which can be done by correcting for the cantilever bending at each point. In order to experimentally obtain a complete force curve using this method, the cantilever spring constant has to be larger than the maximum attractive force gradient. Consequently, a force sensor with low spring constant and high sensitivity will give a large inaccessible region and vice versa.

### 4.3. The force-feedback detector

A way around the problem imposed by the cantilever instability is the implementation of the force-feedback concept<sup>44</sup>. In this type of sensor an external force is acting on the cantilever and the magnitude of this force is controlled by a feedback circuit that maintains the cantilever position as the tip is subjected to the interaction force from the surface. The force on the tip due to the interaction with the surface can then be obtained from the compensating external force and the system should ideally behave as if the cantilever spring constant was infinite. A detailed analysis of the dynamics of the force-feedback system is given in ref. 45. Figure 9 shows an example of a force-feedback sensor that we have implemented in our UHV-AFM. In this kind of system<sup>46</sup>, the end facet of the fiber used for the interferometric detection of the cantilever motion is metalized and electrically connected to a feedback circuit that adjusts the electrostatic attraction imposed on the cantilever to compensate for the tip–surface interaction. As the electrostatic force is always attractive, the cantilever is pre-tensioned in the backward direction by applying a constant bias voltage in order to be able to measure both attractive and repulsive tip forces. We have used this force sensor to investigate the interaction between a Si(111) surface and a tungsten tip. Figure 10 is a

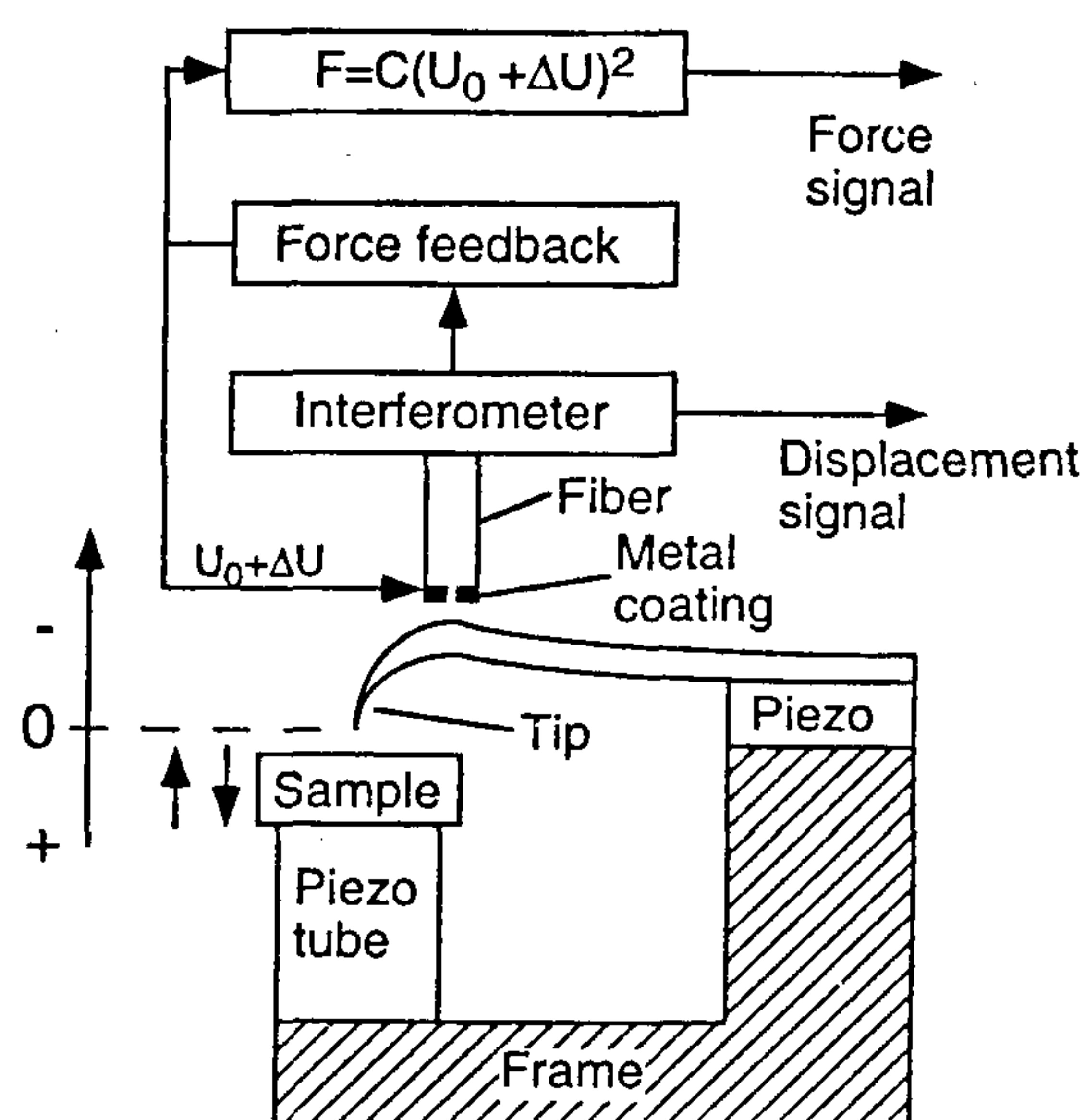


Figure 9. Diagram of the force-feedback instrument equipped with a fiber optic interferometer. The feedback system stabilizes the cantilever position through an attractive electrostatic force resulting from a voltage applied to the metal coated fiber end. Both attraction and repulsion can be measured as the cantilever is pre-tensioned by pulling it back  $\sim 0.2 \mu\text{m}$  by a voltage  $U_0$ . As the actuator force is proportional to  $(U_0 + \Delta U)^2$ , an analogue network is used to convert the controller output  $\Delta U$  to a signal proportional to force.

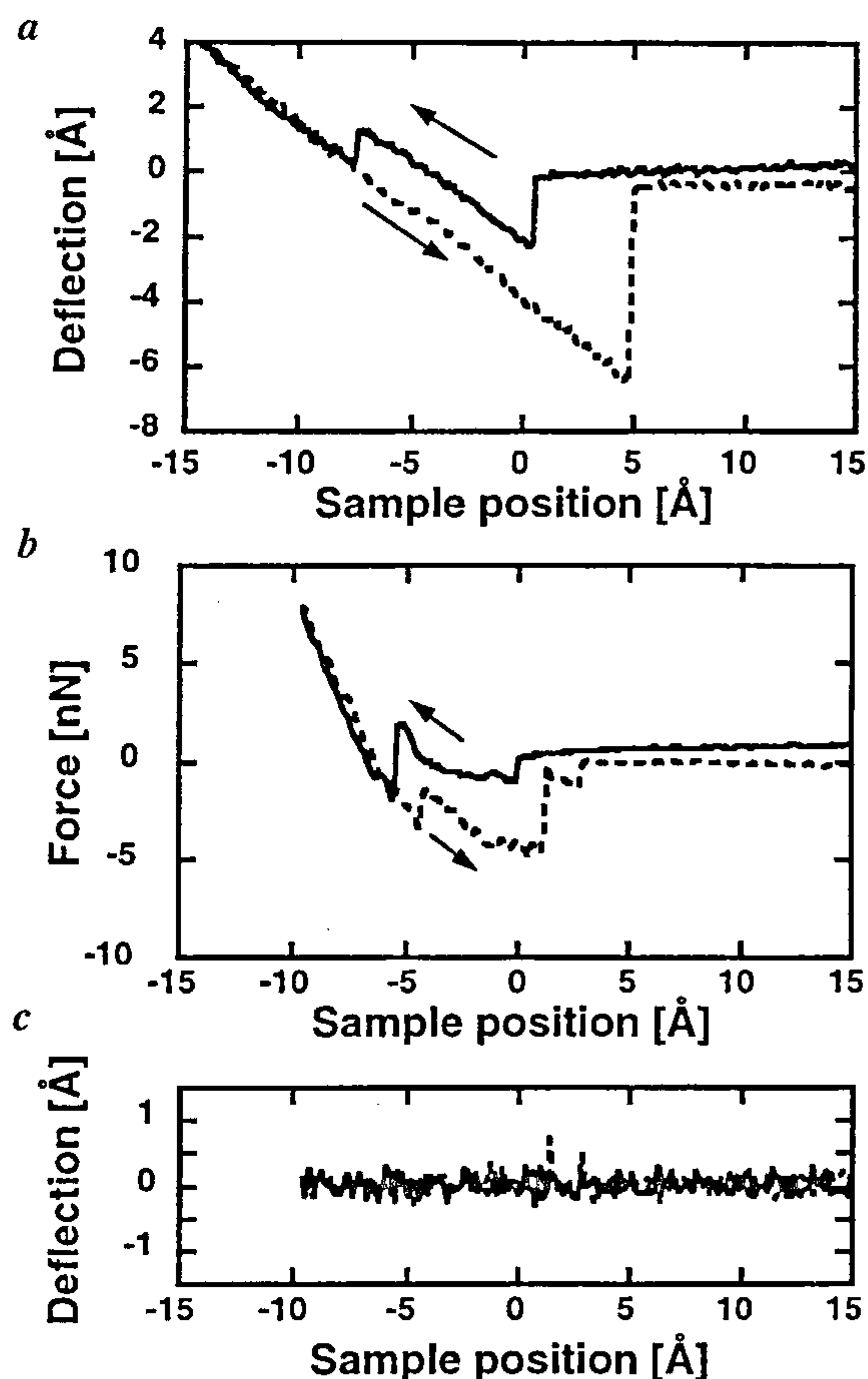


Figure 10. *a*, Cantilever deflection shown as a Si(111) surface is moved in contact and is retracted from a tungsten tip with the force-feedback system disabled. The deflection is transformed to force by multiplication with the spring constant; *b*, Output from the force-feedback system during an approach-retract cycle. *c*, Cantilever deflection during the approach cycle is shown in *b*. As the cantilever remains static, the steps in the force curve in *b* can be attributed to intrinsic events in the tip-surface contact.

comparison between a conventional force curve which shows the cantilever deflection as the sample is moved towards and away from the tip (Figure 10 *a*) and a force curve obtained with the force-feedback activated (Figure 10 *b*). The cantilever deflection during the acquisition of the curve in Figure 10 *b* is presented in Figure 10 *c* which shows that the lever is static in this case, implying that the force signal obtained from the force-feedback circuit corresponds to events in the tip-sample junction rather than cantilever instabilities. The steps observed in Figure 10 *b* correspond to interatomic rearrangements as the tip indents and is pulled away from the surface, which have been predicted by several theoretical calculations<sup>42</sup>.

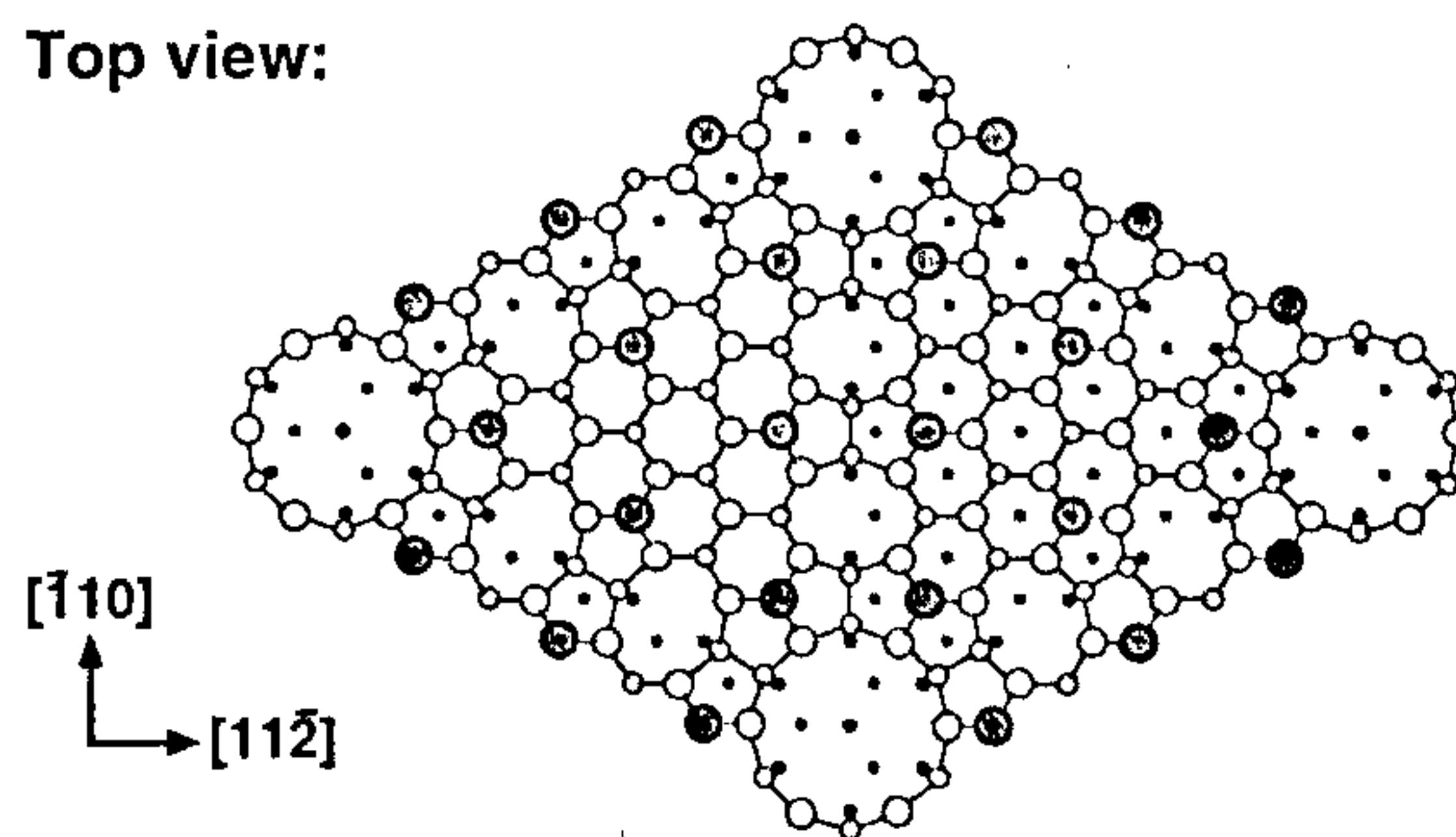
## 5. Force microscopy with atomic resolution

### 5.1. AC-mode imaging using short-range interaction forces

The ac-mode operation of the AFM was originally implemented to measure the weak long-range force, and was later used with high amplitude and repulsive contact for ambient AFM (tapping mode) as described above. In neither case was atomic resolution expected, as the long-range forces are distributed over a large part of the tip, and the repulsive contact during tapping-mode operation is expected to be disruptive to the tip apex. It was thus a major breakthrough when it was first demonstrated that ac-mode AFM in UHV could image with atomic resolution<sup>47</sup>. It is the rapid development of high resolution ac-mode AFM that followed this demonstration that has made AFM a technique capable of investigating surface structure with a resolution comparable to that obtained in STM. As dc-mode imaging of several layered materials had shown contrast with the lattice periodicity due to frictional effects, the capability of the ac-mode instruments to show individual vacancies and steps is sometimes referred to as 'true atomic resolution'.

The sample of choice for the first ac-mode AFM measurements was the Si(111)7×7 reconstructed surface, which was imaged using silicon as well as tungsten tips and using both frequency and amplitude variations of the cantilever oscillation to control the separation<sup>47-50</sup>. Most measurements used oscillation amplitudes of several hundred Å, which means that

#### Top view:



#### Side view:

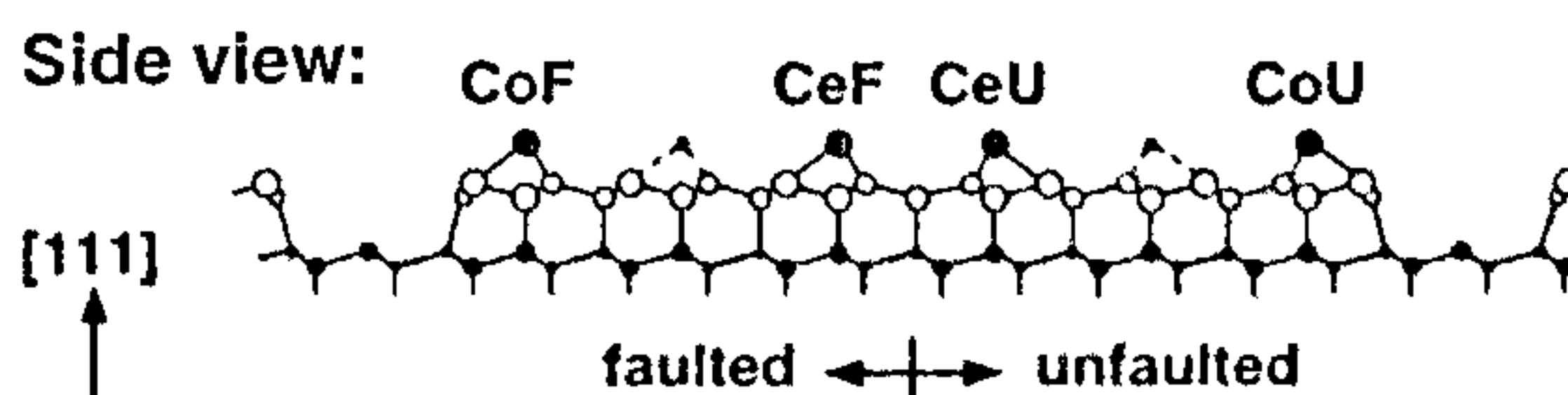


Figure 11. Top and side views of the Si(111)7×7 reconstruction. The adatoms occupy four inequivalent sites denoted by CoF, corner faulted; CeF, centre faulted; CeU, centre unfaulted; and CoU, corner unfaulted.

the observed frequency shift results from the interaction during a small fraction of the oscillation cycle when the tip is at its closest position to the surface. The Si(111)7 × 7 surface is well suited for investigations of the contrast mechanism for several reasons. The unit cell contains 12 atoms projecting further out than the rest, called adatoms, with partially-filled dangling bonds sitting in four electronically inequivalent sites depending on the position in the unit cell (Figure 11). These different sites give different contrasts in STM images depending on whether filled or empty states are probed, which in turn depends on the polarity of the tip<sup>51</sup>. The big unit cell with its adatoms is also easy to identify and a covalent interaction between the tip apex atom and the dangling bonds can be expected to result in a force interaction giving a contrast in AFM. Recently, there have also appeared several theoretical investigations specifically addressing the tip-surface interaction in AFM for this system<sup>52</sup>. After the initial demonstrations of atomically resolved ac-mode imaging of the silicon surface, metals<sup>53</sup>, oxides<sup>54</sup> and a van der Waals surface like graphite (0001)<sup>55</sup> have been imaged with atomic resolution. In order to measure the weak forces from the graphite (0001) surface, the imaging had to be made in an instrument designed for low temperature measurements.

The understanding of the contrast mechanism in high resolution AFM is currently a topic of intense research. As an example of the difference in image contrast between ac-mode AFM and STM we will present the high resolution imaging of the Si(111)7 × 7 reconstruction done in our laboratory<sup>48</sup>.

### 5.2. Example of high resolution ac-mode AFM: Contrast in Si(111)7 × 7 imaging

The Si(111)7 × 7 surfaces were prepared by heat treatment of samples cut from a highly n-doped Si(111) wafer. The AFM image in Figure 12a was obtained using a home-built combined AFM/STM operating in UHV<sup>56</sup>. For AFM imaging, we operate the instrument in the ac-mode using AM-detection. The cantilever/tip units, made from etched tungsten wires, were heat cleaned *in situ* using electron-bombardment. The cantilever/tip used to acquire the AFM image had a resonance frequency of 16.4 kHz, a quality factor of 550, a tip radius estimated to be <150 Å from scanning electron microscopy data, and a spring constant of approximately 60 N/m as estimated from the cantilever geometry.

Figure 12 shows a comparison between an AFM image and a pair of dual-polarity STM images showing the Si(111)7 × 7 reconstruction. Although both the AFM and STM images show the positions of the adatoms, there is an additional contrast between the non-

equivalent corner and centre adatoms in the AFM data. As shown by Pérez *et al.*<sup>52</sup>, the presence of a dangling bond on the apex atom directed towards the surface is expected to have a strong effect on the observed contrast. We have, however, no way of determining whether this atom is a tungsten, oxygen or silicon species.

Figure 12 also shows a cross-section through the raw data along the long diagonal of the 7 × 7 unit cell. This cross-section shows the tip trace above the corner holes and the four inequivalent adatoms, allowing a comparison of the contrast observed in the AFM image with the well-known contrast in filled- and empty-state STM images. In the empty-state STM image there is no contrast between the faulted and unfaulted halves of the unit cell and all the 12 adatoms appear identical. In the filled-states STM images, the corner adatoms appear slightly higher compared to the adjacent centre adatoms and the faulted halves of the unit cell appear slightly higher than the unfaulted halves. The depth of the corner holes in the AFM data (~1 Å) is smaller than the depth observed in the filled- and empty-state STM images (~2 Å). In the cross-section of the AFM image, the difference in apparent height of the corner and centre adatoms is clearly seen. When averaged over several unit cells, the height difference was determined to be 0.13 Å.

In order to correlate the AFM contrast to quantitative details of atomic-scale electronic and structural properties of the surface, it is of crucial importance to understand the ac-mode imaging process. Some insight can be obtained by studying approach curves showing the cantilever deflection (force) and the resonance amplitude as a function of sample position (Figure 13). In these approach curves, recorded after acquiring the image presented in Figure 12a, it can be seen that the oscillation amplitude (initially 16 Å) starts to decrease some 30 Å before the sudden attractive response in the cantilever deflection curve (snap-in) after which the cantilever oscillation is completely damped. To clarify the mechanism behind the observed damping, we recorded the frequency spectra of the cantilever as a function of sample position (Figure 13b). After obtaining a small force-induced frequency shift (curve 2), the sample is moved towards the tip in 3 Å steps. The AFM image shown in Figure 12a was recorded for a constant reduced amplitude of 5 Å compared to the 16 Å free amplitude.

The key question raised by the results presented here is the origin of the atomic contrast observed for the Si(111)7 × 7 reconstruction. This surface has been extensively studied, both experimentally and theoretically, and the exact position of the atom cores as well as the charge in the dangling bonds of the four inequivalent adatoms are well known<sup>57</sup>. The corner adatoms have more charge than the centre adatoms. There is more charge on the adatoms in the faulted half of the unit cell compared to those in the unfaulted half. This is the

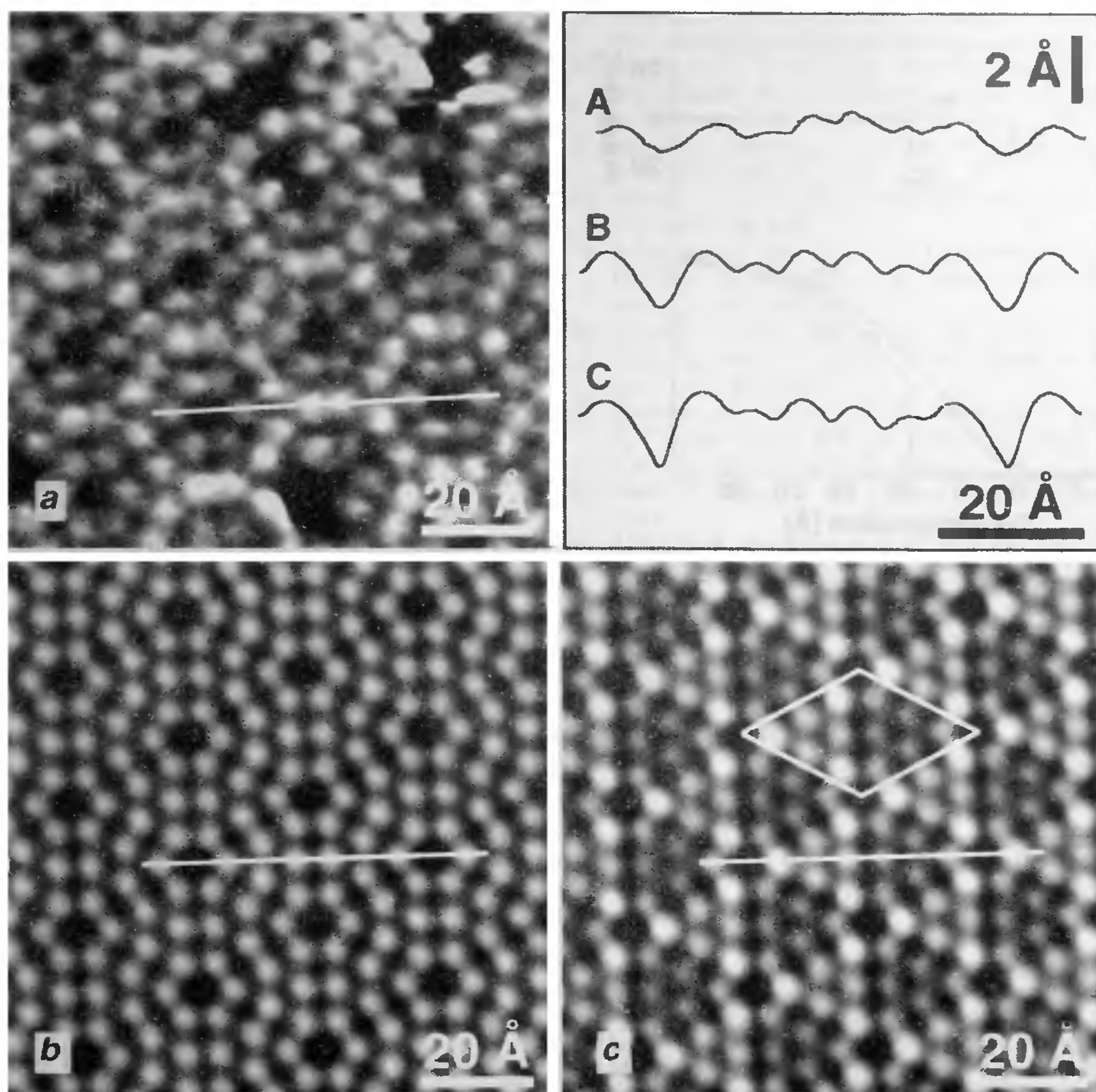


**Figure 12.** Comparison between (a) an AFM image and (b) empty- and (c) filled-state STM images. The grey scales in the images correspond to a height difference of 1 Å. STM images were recorded with tip voltages of  $-2$  V and  $+2.2$  V, respectively, and a constant current of 0.1 nA. The cross-sections through the four inequivalent adatoms are obtained from raw data. The  $7 \times 7$  unit cell is outlined in the filled-state STM image. The faulted and unfaulted halves correspond to the left and right side of the unit cell, respectively.

origin of the contrast observed in filled-state STM images of the surface. Moreover, the vertical position of the adatom cores is directly related to the charge in the dangling bonds such that the adatoms with the most charge are located further away from the surface. However, the height difference between the inequivalent adatoms would correspond to a much smaller contrast than that observed in the filled-state STM image. From Figure 12, it is obvious that the observed AFM contrast neither represents the true ion core positions, nor the charge density in the dangling bond states (the AFM contrast is reversed compared to what would be expected if it reflected these properties).

A property that could contribute to the contrast in AFM images is the chemical reactivity since the tip apex atom is likely to form a bond with a surface atom during each oscillation cycle. Erlandsson and Olsson<sup>58</sup> have simulated the variation in the cantilever resonance curves using a Morse potential for the atom–atom interaction, and have shown that binding energy variations of 1 eV produce variations that could create a significant contrast, supporting the assumption that the observed contrast is of chemical origin. These simulations also show that frequency variations related to the short-range chemical forces can occur without the tip entering the repulsive interaction region. Chemical reactivity is not a

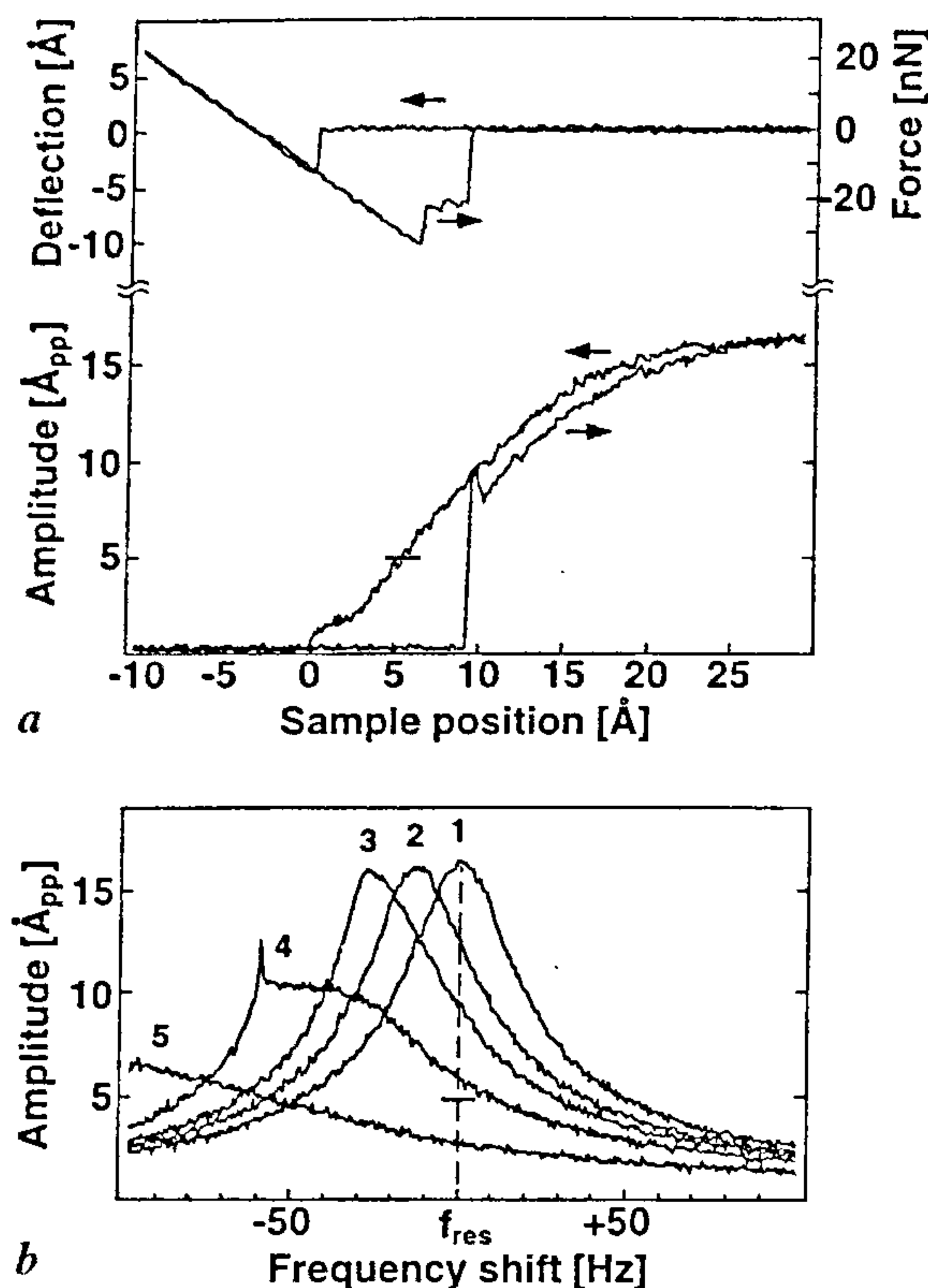


**Figure 13.** *a*, Deflection of the cantilever (upper curve) and the peak to peak oscillation amplitude (lower curve) as a function of sample position. Zero on the horizontal axis is defined as the point of initial hard contact and negative numbers correspond to contact. The force scale only gives approximate values as the spring constant of the cantilever is not precisely known. The applied oscillation in the cantilever deflection signal is not seen since it was lowpass filtered with a cut-off frequency of 100 Hz. The horizontal bar intersecting the amplitude curve indicates the operating point (5 Å); *b*, A series of resonance spectra of the cantilever for different tip to sample separations. Curve 1 was recorded at a separation where no force was detected, giving the resonance frequency of the undisturbed oscillation. Curves 2–5 were recorded for sample positions corresponding to 12, 15, 18 and 21 Å with respect to curve 1, moving the sample towards the tip. The horizontal scale shows the deviation from the undisturbed resonance frequency. The horizontal bar intersecting the line showing the undisturbed resonance frequency indicates the operating point (5 Å).

well-defined property of the surface atoms themselves as it also depends on the reacting species. In several of the cases studied experimentally using other methods, the trend is, however, that the centre adatoms are more reactive than the corner adatoms<sup>59</sup>, in agreement with the AFM contrast we observe.

Details of the contrast effects like these shown here are not well understood at present and other groups have also observed contrast variations when imaging the Si(111)7 × 7 surface in ac-mode AFM that have been

shown to vary with imaging parameters<sup>60</sup>. A general problem when interpreting data of this kind is the lack of knowledge of the atom species at the tip apex as sample material might be picked up by the tip and the precise orientation of the orbitals of the tip atom can have strong effects on the resolution. Improvement of *in situ* tip characterization methods like Field Ion Microscopy (FIM) is one important step that should help us understand the contrast mechanism in high resolution AFM even better.

## 6. Future trends

As the ac-mode AFM is becoming a routine tool for high resolution imaging, the whole class of insulators that has not been possible to image with the STM can now be investigated with atomic resolution. As we learn more about the interaction mechanism in high resolution ac-mode force microscopy, there is the future possibility that one may be able to directly investigate the chemical bonding forces, and atomically resolved force spectroscopy will become an important method that will complement the locally obtained electronic information which is obtained using tunnelling spectroscopy. The combination of atomically resolved AFM and sensors based on the force-feedback concept will soon make direct measurements of interatomic binding forces possible. We can expect future instruments to combine AFM with STM to provide a versatile surface science tool, that will also make it possible to clarify the exact origin of the force induced artifacts in tunnelling microscopy. Within the biological field, where the AFM is extensively used due to its ability to operate in liquids, we can expect an improved ability to image at the molecular level combined with the use of functionalized tips that can probe antibody–antigen interactions as well as forces related to protein folding. The development of special types of force microscopes capable of measurements of individual magnetic spin-sites is moving rapidly forward<sup>61</sup>, and we can expect powerful techniques like ESR and NMR that now use macroscopic sample volumes to develop into site-specific methods that can add chemical specificity to atomically resolved probe microscopy.

1. Binnig, G., Quate, C. F. and Gerber, Ch., *Phys. Rev. Lett.*, 1986, **56**, 930.
2. Binnig, G., Rohrer, H., Gerber, Ch. and Weibel, H., *Phys. Rev. Lett.*, 1982, **49**, 57.
3. Young, R., Ward, J. and Scire, F., *Rev. Sci. Instrum.*, 1972, **43**, 999.
4. Wiesendanger, R., *Scanning Probe Microscopy and Spectroscopy, Methods and Applications*, Cambridge University Press, 1994, *Scanning Tunnelling Microscopy I, II and III* (eds Wiesendanger, R. and Güntherodt, H. J.), Springer-Verlag, Berlin.

5. Terris, B. D., Stern, J. E., Rugar, D. and Mamin, H. J., *Phys. Rev. Lett.*, 1989, **63**, 2669; Rugar, D., Mamin, H. J., Guethner, P., Lambert, S. E., Stern, J. E., McFadyen, I. and Yogi, T., *J. Appl. Phys.*, 1990, **68**, 1169; Nonnenmacher, M., O'Boyle, M. P. and Wickramasinghe, H. K., *Appl. Phys. Lett.*, 1991, **58**, 2921.
6. Matey, J. R. and Blanc, J., *J. Appl. Phys.*, 1985, **57**, 1437.
7. Williams, C. and Wickramasinghe, H. K., *Appl. Phys. Lett.*, 1986, **49**, 1587.
8. Hansma, P. K., Drake, B., Marti, O., Gould, S. A. C. and Prater, C. B., *Science*, 1989, **243**, 641.
9. Guethner, P., Fischer, U. Ch. and Dransfeld, K., *Appl. Phys. B*, 1989, **48**, 89.
10. Pohl, D. W., Denk, W. and Lanz, M., *Appl. Phys. Lett.*, 1984, **44**, 651.
11. Hartmann, U., *J. Vac. Sci. Technol.*, 1991, **B9**, 465; Johansson, P. and Apell, P., *Phys. Rev. B*, 1997, **56**, 4159.
12. Israelachvili, J. N., *Intermolecular and Surface Forces*, Academic Press, London, 1991, 2nd edn, pp. 176–212.
13. Hamaker, H. C., *Physica (Amsterdam)*, 1937, **4**, 1058.
14. Derjagin, B. V., *Kolloid Z.*, 1934, **69**, 155.
15. Andersson, Y., Hult, E., Apell, P., Langreth, D. C. and Lundqvist, B. I., *Solid State Commun.*, 1998, **106**, 235.
16. White, L. R., *J. Colloid. Interface Sci., Physica*, 1983, **95**, 286.
17. Olsson, L., Lin, N., Yakimov, V. and Erlandsson, R., *J. Appl. Phys.*, 1998, **84**, 4060.
18. Domansky, K., Leng, Y., Williams, C. C., Janata, J. and Petelenz, D., *Appl. Phys. Lett.*, 1993, **63**, 1264.
19. Grütter, P., Mamin, H. J. and Rugar, D., in *Scanning Tunnelling Microscopy II* (eds Wiesendanger, R. and Güntherodt, H. J.), Springer-Verlag, Berlin, 1995.
20. Hellman, H., *Einführung in Quanten Theorie*, Deutsch, Leipzig 1937; Feynman, R. P., *Phys. Rev.*, 1939, **56**, 340.
21. Ciraci, S., Baratoff, A. and Batra, I. P., *Phys. Rev. B*, 1990, **41**, 2763.
22. Chen, C. J., *J. Phys. Condens Matter*, 1991, **3**, 1227.
23. Lennard-Jones, J. E. and Dent, B. M., *Trans. Faraday Soc.*, 1928, **24**, 92.
24. Slater, J. C., *Quantum Theory of Molecules and Solids*, McGraw-Hill, New York, 1963, vol. 1, pp. 17–19.
25. Martin, Y., Williams, C. C. and Wickramasinghe, H. K., *Scanning Microsc.*, 1988, **2**, 3; Ducker, W. A., Cook, R. F. and Clarke, D. R., *J. Appl. Phys.*, 1990, **67**, 4045.
26. Soler, J. M., Baro, A. M., Garcia, N. and Rohrer, H., *Phys. Rev. Lett.*, 1986, **57**, 444.
27. Chen, C. J. and Hamers, R. J., *J. Vac. Sci. Technol.*, 1991, **B9**, 503.
28. Dürig, U., Züger, O. and Pohl, D. W., *Phys. Rev. Lett.*, 1990, **65**, 349.
29. Crommie, M. F., Lutz, C. P. and Eigler, D. M., *Science*, 1993, **262**, 218.
30. Meyer, G. and Amer, N. M., *Appl. Phys. Lett.*, 1988, **53**, 1045.
31. Rugar, D., Mamin, H. J., Erlandsson, R., Stern, J. E. and Terris, B. D., *Rev. Sci. Instrum.*, 1988, **59**, 2337.
32. Villarubbia, J. S., *J. Res. Natl. Inst. Stand. Technol.*, 1997, **102**, 425.
33. Giessibl, F. J. and Binnig, G., *Ultramicroscopy*, 1992, **42–44**, 281; Ohnesorge, F. and Binnig, G., *Science*, 1993, **260**, 1451; Schimmel, Th., Koch, Th., Küppers, J. and Lux-Steiner, M., *Appl. Phys. A*, 1999, **68**, 399.
34. Pethica, J. B. and Sutton, P., *J. Vac. Sci. Technol. A*, 1988, **6**, 2490.
35. Mate, C. M., McClelland, G. M., Erlandsson, R. and Chiang, S., *Phys. Rev. Lett.*, 1987, **59**, 1942.
36. Tománek, D., in *Scanning Tunnelling Microscopy III* (eds Wiesendanger, R. and Güntherodt, H. J.), Springer-Verlag, Berlin, 1996.
37. Martin, Y., Williams, C. C. and Wickramasinghe, H. K., *J. Appl. Phys.*, 1987, **61**, 4723.
38. Albrecht, T. R., Grutter, P., Horne, D. and Rugar, D., *J. Appl. Phys.*, 1991, **69**, 668.
39. Erlandsson, R. and Olsson, L., *Appl. Phys. A*, 1998, **66**, 879; Gotsmann, B., Anczykowski, B., Seidel, C. and Fuchs, H., *Appl. Surf. Sci.*, 1999, **140**, 314.
40. Giessibl, F. J., *Phys. Rev. B*, 1997, **56**, 16010.
41. Zong, Q., Innis, D., Kjoller, K. and Elings, V. B., *Surf. Sci. Lett.*, 1993, **290**, L688.
42. Landman, U., Luedtke, W. D., Burnham, N. A. and Colton, R. J., *Science*, 1990, **248**, 454; Buldum, A., Ciraci, S. and Batra, I. P., *Phys. Rev. B*, 1998, **57**, 2468.
43. Rubio, G., Agrait, N. and Vieira, S., *Phys. Rev. Lett.*, 1996, **76**, 2302.
44. Joyce, S. A. and Houston, J. E., *Rev. Sci. Instrum.*, 1991, **62**, 710; Jarvis, S. P., Dürig, U., Lanz, M. A., Yamada, H. and Tokumoto, H., *Appl. Phys. A*, 1998, **66**, S211.
45. Stewart, A. M. and Parker, J. L., *Rev. Sci. Instrum.*, 1992, **63**, 5626; Kato, N., Kikuta, H., Nakano, T., Matsumoto, T. and Iwata, K., *Rev. Sci. Instrum.*, 1999, **70**, 2402.
46. Kato, N., Suzuki, I., Kikuta, H. and Iwata, K., *Rev. Sci. Instrum.*, 1997, **68**, 2475.
47. Giessibl, F. J., *Science*, 1995, **267**, 69.
48. Erlandsson, R., Olsson, L. and Mårtensson, P., *Phys. Rev. B*, 1996, **54**, R8309.
49. Kitamura, S. and Iwatsuki, M., *Jpn. J. Appl. Phys.*, 1995, **34**, L145.
50. Güthner, P., *J. Vac. Sci. Technol. B*, 1996, **14**, 2428.
51. Hamers, R. J., Tromp, R. M. and Demuth, J. E., *Phys. Rev. Lett.*, 1986, **56**, 1972.
52. Perez, R., Payne, M., Stich, I. and Terakura, K., *Phys. Rev. Lett.*, 1997, **78**, 678; Pérez, R., Stich, I., Payne, C. and Terakura, K., *Phys. Rev. B*, 1998, **58**, 10835.
53. Orisaka, S., Minobe, T., Uchihashi, T., Sugawara, Y. and Morita, S., *Appl. Surf. Sci.*, 1999, **140**, 243.
54. Fukui, K., Onishi, H. and Iwasawa, Y., *Appl. Surf. Sci.*, 1999, **140**, 259; Raza, H., Pang, C. L., Haycock, S. A. and Thornton, G., *Appl. Surf. Sci.*, 1999, **140**, 271.
55. Allers, W., Schwarz, A., Schwarz, U. D. and Wiesendanger, R., *Appl. Surf. Sci.*, 1999, **140**, 247.
56. Olsson, L., Wigren, R. and Erlandsson, R., *Rev. Sci. Instrum.*, 1996, **67**, 2289.
57. Brommer, K. D., Larson, B. E., Needels, M. and Joannopoulos, J. D., *Jpn. J. Appl. Phys.*, 1993, **32**, 1360; Stich, I., Payne, M. C., King-Smith, R. D., Lin, J.-S. and Clarke, L. J., *Phys. Rev. Lett.*, 1992, **68**, 1351.
58. Erlandsson, R. and Olsson, L., *Appl. Phys. A*, 1998, **66**, S879.
59. Shimomura, M., Sanada, N., Fukuda, Y. and Moller, P. J., *Surf. Sci.*, 1995, **341**, L1061; Jensen, J. A., Jan, C. and Kummel, A. C., *Phys. Rev. Lett.*, 1996, **76**, 1388.
60. Nakagiri, N., Suzuki, M., Okiguchi, K. and Sugimura, H., *Surf. Sci.*, 1997, **373**, L329; Uchihashi, T., Sugawara, Y., Tsukamoto, T., Ohto, M. and Morita, S., *Phys. Rev. B*, 1997, **56**, 9834.
61. Zuger, O., Hoen, S. T., Yannoni, C. S. and Rugar, D., *J. Appl. Phys.*, 1996, **79**, 1881.